# Use of Tissue Water as a Concentration Reference for Proton Spectroscopic Imaging

Charles Gasparovic,[1,2]* Tao Song,[8] Deidre Devier,[5] H. Jeremy Bockholt,[6] Arvind Caprihan,[7] Paul G. Mullins,[1,3] Stefan Posse,[4,6] Rex E. Jung,[3,5,6] and Leslie A. Morrison[3]

A strategy for using tissue water as a concentration standard in ^{1}H magnetic resonance spectroscopic imaging studies on the brain is presented, and the potential errors that may arise when the method is used are examined. The sensitivity of the method to errors in estimates of the different water compartment relaxation times is shown to be small at short echo times (TEs). Using data from healthy human subjects, it is shown that different image segmentation approaches that are commonly used to account for partial volume effects (SPM2, FSL's FAST, and K-means) lead to different estimates of metabolite levels, particularly in gray matter (GM), owing primarily to variability in the estimates of the cerebrospinal fluid (CSF) fraction. While consistency does not necessarily validate a method, a multispectral segmentation approach using FAST yielded the lowest intersubject variability in the estimates of GM metabolites. The mean GM and white matter (WM) levels of N-acetyl groups (NAc, primarily N-acetylaspartate), choline (Ch), and creatine (Cr) obtained in these subjects using the described method with FAST multispectral segmentation are reported: GM [NAc] = 17.16 ± 1.19 mM; WM [NAc] = 14.26 ± 1.38 mM; GM [Ch] = 3.27 ± 0.47 mM; WM [Ch] = 2.65 ± 0.25 mM; GM [Cr] = 13.98 ± 1.20 mM; and WM [Cr] = 7.10 ± 0.67 mM.   Magn Reson Med 55: 1219–1226, 2006. © 2006 Wiley-Liss, Inc.

Key words: ^{1}H-MRS; tissue water; spectroscopic imaging; relaxation times; voxel

The unsuppressed "internal" water signal was introduced as a concentration reference for single-voxel proton magnetic resonance spectroscopy (^{1}H-MRS) of the brain over a decade ago (1–4). However, to our knowledge, a detailed description of how this method could be applied to spectroscopic imaging (SI), or an examination of its potential sources of error has yet to be reported. In the majority of SI studies that reported "absolute" metabolite concentrations, the metabolite signals were converted to moles per liter or kilograms of tissue using either external metabolite solutions (5–7) or ventricle water (8,9), and relatively few groups have reported using internal water (10,11). The principal advantage of using internal water in SI studies is that certain factors and potential sources of error that need to be considered when using external concentration references (e.g., RF homogeneity, coil loading, or the SI point spread function (PSF)) are obviated, since the water and metabolite signals come from the same voxel and are acquired in essentially the same way.

The major assumptions when using internal water, on the other hand, are that the water densities and signal relaxation times of gray matter (GM), white matter (WM), and cerebrospinal fluid (CSF) in the region of interest (ROI) can be reliably estimated and, furthermore, do not change significantly among the studied groups. Moreover, it is essential that the volume fractions of these tissues and CSF in each SI voxel are accurately measured. Measuring partial volume effects is also a requirement when using external referencing methods, but the demand on accuracy is greater when using internal water. This is because only the signal from the combined GM-WM fraction of the total water, in which the detectable metabolites are exclusively located, is used as the concentration reference. The observed water signal, however, arises from a combination of the GM, WM, and CSF water fractions, each of which is weighted by different relaxation times. Thus, an accurate estimate of the parenchymal water signal relies on an accurate assessment of the relaxation-weighted signals from all compartments—not simply the CSF compartment, as is done with methods using external references. Estimating the combined GM-WM and CSF fractions with relaxation experiments, as introduced by Ernst et al. (1) for single-voxel MRS, is not practical for SI studies, nor can the separate GM and WM fractions be assessed in this way. The standard means for estimating not only the CSF fraction but the separate GM and WM fractions in SI studies, therefore, has been by image segmentation.

In this article we present a strategy for using internal water as a concentration standard in SI studies, drawing on previous reports by others on single-voxel MRS (1–4,12) as well as SI methods using other concentration standards (13). Next we examine the potential errors that may arise when using this method, first with simulated data based on given fractions and relaxation times of the

[1]MIND Imaging Center, University of New Mexico, Albuquerque, New Mexico, USA.

[2]Department of Neurosciences, University of New Mexico, Albuquerque, New Mexico, USA.

[3]Department of Neurology, University of New Mexico, Albuquerque, New Mexico, USA.

[4]Department of Psychiatry, University of New Mexico School of Medicine, Albuquerque, New Mexico, USA.

[5]Department of Psychology, University of New Mexico, Albuquerque, New Mexico, USA.

[6]MIND Institute, Albuquerque, New Mexico, USA.

[7]New Mexico Resonance, Albuquerque, New Mexico, USA.

[8]Department of Radiology, University of California–San Diego, San Diego, California, USA.

*Correspondence to: Charles Gasparovic, Ph.D., MIND Imaging Center, University of New Mexico, Health Sciences Center, 1101 Yale Blvd. NE, Albuquerque, NM 87131. E-mail: chuck@unm.edu

various water compartments, and then with data from human subjects submitted to three commonly used image segmentation routines: 1) a K-means algorithm implemented by IMGCON software (www.fmrib.ox.ac.uk), 2) a mixture model cluster analysis algorithm (14) implemented by the Statistical Parametric Mapping (SPM2) software (www.fil.ion.ucl.ac.uk/spm), and 3) FSL's FAST segmentation routine (www.fmrib.ox.ac.uk/fsl/fast) based on a hidden Markov random field model and an associated expectation-maximization algorithm (15). Finally, we report estimates of GM and WM levels of choline (Ch), creatine (Cr), and N-acetyl groups (NAc, N-acetylaspartate (NAA) and N-acetylaspartylglutamate (NAAG)) in these subjects based on FAST multispectral segmentation.

## THEORY

The standard approach to using the tissue water signal as an internal concentration reference assumes that the fully relaxed signal from water or any metabolite in the spectroscopic voxel will be proportional to the number of moles of the molecule in the voxel. Since CSF contains no observable metabolites, the water signal in which we are interested arises only from the GM and WM tissue fractions of the voxel. Also, since the water and metabolite signals originate from the same voxel and are acquired with the same sequence, we can write

$$\frac{S_{M\_R}}{S_{H2O\_GM/WM\_R}} = \frac{\text{Moles}_M \times \#H_M}{\text{Moles}_{H2O\_GM/WM} \times 2} \quad [1]$$

where the subscripts refer to water ($H_2O$) or metabolite (M) in the parenchyma (GM/WM) of the voxel, R refers to the fact that the magnetization of the protons is fully relaxed, $\#H_M$ is the number of protons that give rise to the metabolite peak of interest, and 2 is the number of water protons. If we assume that the metabolites and water come from the same "wet" volume of the voxel, we may write

$$[M] = \frac{S_{M\_R}}{S_{H2O\_GM/WM\_R}} \times \frac{2}{\#H_M} \times [H_2O] \quad [2]$$

where $[H_2O]$ denotes the molal concentration (moles/kilogram of solvent) of MR-visible water in the metabolite solution (2,16) of the parenchyma, which is assumed here to be that of pure water (55.51 mol/kg).

The expression for the concentration reference intensity $S_{H2O\_GM/WM\_R}$ is derived from the observed water signal $S_{H2O\_obs}$ by noting that this signal is related to the fully relaxed total water signal $S_{H2O\_R}$ according to the expression

$$S_{H2O\_obs} = f_{GM} \times S_{H2O\_R} \times R_{H2O\_GM}$$
$$+ f_{WM} \times S_{H2O\_R} \times R_{H2O\_WM} + f_{CSF} \times S_{H2O\_R} \times R_{H2O\_CSF} \quad [3]$$

where $f_{GM}$, $f_{WM}$, and $f_{CSF}$ are the fractions of water attributable to GM, WM, and CSF, respectively. The various relaxation attenuation factors are given by $R_{H2O\_y} = \exp[-TE/T2_{H2O\_y}](1 - \exp[-TR/T1_{H2O\_y}])$, where $T1_{H2O\_y}$ and $T2_{H2O\_y}$ are the $T_1$ and $T_2$ relaxation times of water in compartment y, TE is the sequence echo time, and TR is

the repetition time. To obtain $S_{H2O\_GM/WM\_R}$, we solve for $S_{H2O\_R}$ and subtract from it the fraction that is CSF:

$$S_{H2O\_GM/WM\_R} =$$
$$\frac{S_{H2O\_obs}(1 - f_{CSF})}{f_{GM} \times R_{H2O\_GM} + f_{WM} \times R_{H2O\_WM} + f_{CSF} \times R_{H2O\_CSF}} \quad [4]$$

Note that the fractions in Eqs. [3] and [4] are the molal water fractions. They can be related to the volume fractions of GM, WM, and CSF determined by image segmentation by taking into account the relative water fraction in each segmentation fraction. Assuming that the relative densities of MR-visible water in GM, WM, and CSF are 0.78, 0.65, and 0.97 (1), respectively:

$$f_{GM} = \frac{f_{GM\_vol} \times 0.78}{f_{GM\_vol} \times 0.78 + f_{WM\_vol} \times 0.65 + f_{CSF\_vol} \times 0.97} \quad [5]$$

$$f_{WM} = \frac{f_{WM\_vol} \times 0.65}{f_{GM\_vol} \times 0.78 + f_{WM\_vol} \times 0.65 + f_{CSF\_vol} \times 0.97} \quad [6]$$

and

$$f_{CSF} = \frac{f_{CSF\_vol} \times 0.97}{f_{GM\_vol} \times 0.78 + f_{WM\_vol} \times 0.65 + f_{CSF\_vol} \times 0.97} \quad [7]$$

where the fractions $f_{GM\_vol}$, $f_{WM\_vol}$, $f_{CSF\_vol}$ are the GM, WM, and CSF volumes, respectively, determined by segmentation. It is worth noting that an approximation of $S_{H2O\_GM/WM\_R}$ simply as $S_{H2O\_obs}(1-f_{csf\_vol})$ divided by a mean relaxation attenuation factor for parenchyma may substantially overestimate $S_{H2O\_GM/WM\_R}$ and thus underestimate the metabolite values. This will be particularly true at long TE (>30 ms) and short TR (<6 s) and in voxels with significant CSF, owing to the much longer relaxation times of the CSF water magnetization and hence the greater attenuation of its signal relative to the GM and WM signals.

Using the approach taken in SI studies with external concentration references (9), the relaxation attenuation of the fully relaxed metabolite signal $S_{M\_R}$ can be estimated from the mean $T_1$ and $T_2$ values of the metabolite protons since, unlike water in GM, WM, and CSF, these values do not appear to differ substantially in GM and WM (17–19). Hence, $S_{M\_R} \approx S_{M\_obs}/R_m$, where $R_M = \exp[-TE/T2_{M\_ave}](1 - \exp[-TR/T1_{M\_ave}])$ and, combining Eqs. [2] and [4], we obtain

$$[M] =$$
$$\frac{S_{M\_obs} \times (f_{GM} \times R_{H2O\_GM} + f_{WM} \times R_{H2O\_WM} + f_{CSF} \times R_{H2O\_CSF})}{S_{H2O\_obs}(1 - f_{CSF}) \times R_M}$$
$$\times \frac{2}{\#H_M} \times [H_2O] \quad [8]$$

To obtain the concentration of a metabolite in either "pure" GM or WM, one can apply the statistical regression

FIG. 1. Deviations of the estimated parenchymal water proton signal strength (S) from the true relaxation-corrected signal strength (equal to a relative value of 80) due to errors in the water proton $T_1$ or $T_2$ values used in Eq. [8], as a function of fractional GM at a fixed CSF fraction of 0.2 (see text for details). Each plot in the left column shows deviations due to errors of 0%, $\pm$10%, $\pm$20%, and $\pm$30% in the $T_2$ of either the GM, WM, or CSF water protons (indicated in the far left column) at different TR and TE values (indicated in the far right column). The right column of plots similarly shows deviations due to errors in $T_1$. The outer lines of selected plots are labeled –30% or +30% to indicate the directions of the errors with increasingly negative or positive deviations, respectively, from the assumed correct $T_1$ or $T_2$ values.
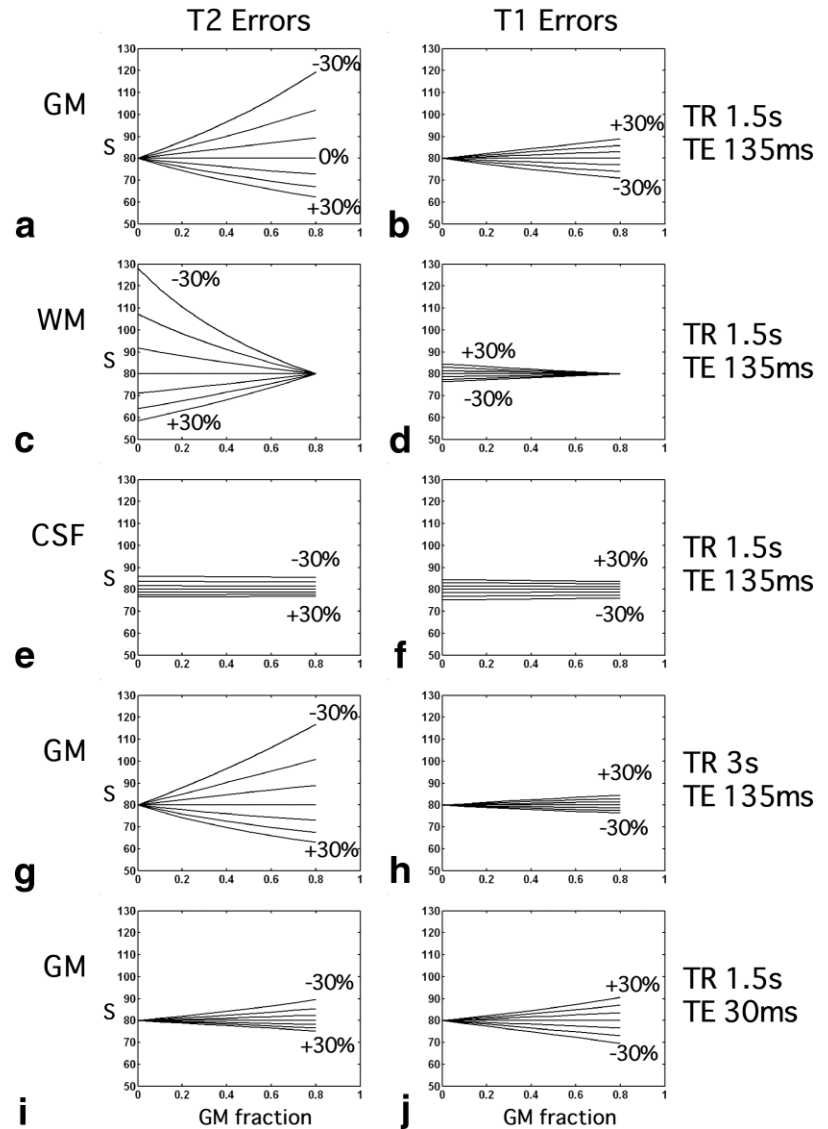
method of Hetherington et al. (9) to the plot of [M] vs. fractional GM in the parenchyma, extrapolating the regression line to GM = 1 to estimate the concentration in pure GM, and to GM = 0 to estimate the value in pure WM (Fig. 3).

### Estimates of the Error due to Inaccurate Relaxation Times

The major potential sources of error in Eq. [8], aside from those inherent to acquiring the MRS signals and the estimate of the metabolite relaxation attenuation factor common to all methods, are the estimates of the various tissue and CSF fractions of water and relaxation times associated with them. We begin by examining the potential errors due to inaccurate estimates of the water proton $T_1$ and $T_2$ times in GM, WM, and CSF, which, judging from the range of values reported in the literature for normal-appearing tissue alone (20,21), may differ by 10% or more from the true relaxation times. Furthermore, increases in water relaxation times in regions of edema, tumor, plaque, or other types of brain lesions may be as high as 20% or more (22,23).

To this end, we altered the $T_1$ or $T_2$ values used to calculate $S_{H2O\_GM/WM\_R}$ by 0 to $\pm$30% in steps of 10% from values at 1.5T found in published reports (GM: $T_1$ = 1.304, $T_2$ = 0.093 (20); WM: $T_1$ = 0.660, $T_2$ = 0.073 (20,22); CSF: $T_1$ = 2.93, $T_2$ = 0.23 (22)). Figure 1 displays a sample of the results of such an analysis based on a TR of 1.5 s, a TE of 135 ms, and an $f_{CSF}$ of 0.2 (a fraction of CSF that might be encountered in SI voxels along the interhemispheric midline in a typical transverse SI slice above the lateral ventricles). Evident in these plots is the relatively high sensitivity of the estimates to errors in GM or WM water $T_2$, which scale nearly linearly with the fraction of GM or WM, respectively. The sensitivity to WM water $T_1$ error is less than that to GM water $T_1$ error, owing to the much shorter $T_1$ of water in WM, and errors in the CSF relaxation parameters lead to only small errors in the estimate of $S_{H2O\_GM/WM\_R}$ due to the relatively long $T_2$ and low fraction of CSF water protons in this example. It would not be practical to show every permutation of the errors in the six relaxation times over a range of TE, TR, and CSF fractions, but the major implications of such an
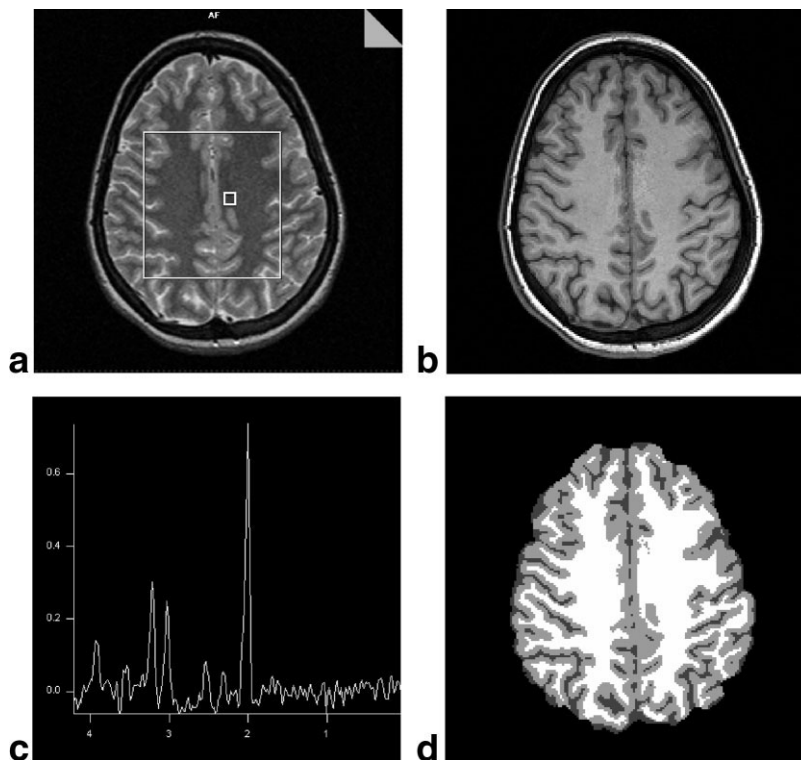
FIG. 2. Sample data from one subject. **a:** $T_2$-weighted image in the center of the SI slice, indicating the PRESS excitation volume (large rectangle) and voxel location of the spectrum shown in **c** (small rectangle). **b:** Corresponding $T_1$-weighted image. **d:** Result of segmentation of $T_1$-weighted image using FSL's FAST.

analysis can be drawn from these plots. Generally, and as expected, simultaneous errors in the various relaxation times will have either cumulative or offsetting effects depending on the direction of the error. Also, this sensitivity is greatly reduced at short TE (Fig. 1i and j). On the other hand, lengthening the TR (Fig. 1g, h) reduces the sensitivity to $T_1$ errors, but from a level that was relatively low to begin with. Since lengthening the TR undesirably lengthens the total SI scan time, while shortening the TE does not, the strategy suggested by this analysis for reducing sensitivity to relaxation time errors when using water as an internal reference is to acquire the data with the shortest TE possible.

## Comparison of Segmentation Methods With Data From Human Subjects

As a practical demonstration of the sensitivity of the internal water referencing method to errors in the measured
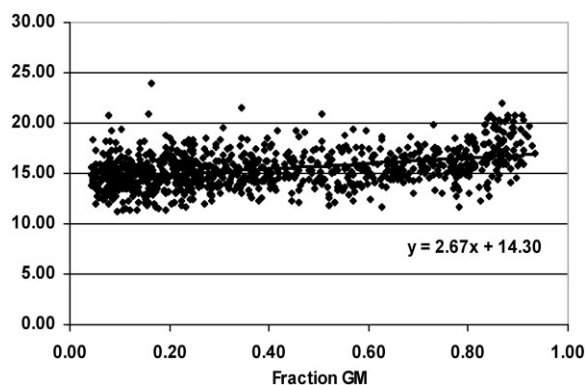


FIG. 3. Example of regression analysis for [NAA] and fractional GM ($f_{gm}/(f_{gm}+f_{wm})$) as determined by FAST multispectral segmentation. Data from all 14 subjects in the study were pooled.

water compartment fractions, we analyzed SI and image data from 14 normal subjects who participated in an ongoing study on myotonic dystrophy at the University of New Mexico Health Sciences Center. Three different methods were used to segment either the $T_1$- or $T_2$-weighted images alone or a combination of both image data sets using a multispectral approach. The spectroscopic data were acquired with a pulse sequence and TE that are commonly used in routine clinical SI, using point-resolved spectroscopy (PRESS) localization with a TE of 135 ms. While this TE is relatively long and makes the data analysis more prone to relaxation errors than would the use of shorter values, it is intermediate between typical short ($\leq$30 ms) and long (270–280 ms) TEs and yields a relatively flat spectral baseline. The latter feature is desirable for accurate curve-fitting of the data when only the major singlet peaks are of interest. The results of the different approaches are compared with respect to the ratio of GM [NAc] to WM [NAc] derived from regression analyses of the data ([NAc] as a function of fractional parenchymal GM). We examined the variability among the different methods by performing regression analyses on both the pooled subject data and the data from individual subjects.

## MATERIALS AND METHODS

### Subjects

Fourteen adult subjects (six males and eight females) with no evidence of neurological defects were scanned after they provided written informed consent, in accordance with a protocol approved by the Human Research Review Committee of the University of New Mexico Health Sciences Center.

## MR Acquisition Methods

MRI and SI were performed on a 1.5-T Sonata scanner (Siemens) using a circularly polarized head coil. Sagittal scout images were obtained to prescribe $T_1$- and $T_2$-weighted images perpendicular to the interhemispheric midline and angled parallel to a line drawn through the anterior (AC) and posterior (PC) commissures. $T_1$-weighted images were obtained with a 3D fast low-angle shot (FLASH) sequence (TR/TE = 20/5.86 ms, flip angle = 25°, field of view (FOV) = 200 × 200 mm, matrix = 192 × 192, slice thickness = 1.5 mm, total scan time = 14 min 22 s), and $T_2$-weighted images were obtained with a turbo spin-echo (TSE) sequence (TR/TE = 9700/50 ms, turbo factor = 5, FOV = 200 × 200 mm, matrix = 192 × 192, slice thickness = 1.5 mm, total scan time = 6 min 10 s).

SI was performed with a phase-encoded version of a PRESS sequence with or without water presaturation (TR/TE = 1500/135 ms, FOV = 200 × 200 mm, slice thickness = 15 mm, circular $k$-space sampling (radius = 24), total scan time = 9 min 42 s). The nominal voxel size was $6.25 \times 6.25 \times 15$ mm$^3$ after zero-filling in $k$-space to 32 × 32 samples. Both water-suppressed and -unsuppressed data sets were collected. The SI volume of interest (VOI) established by the PRESS volume-selection gradients was prescribed with an FSE image to lie immediately above the lateral ventricles and parallel to the AC-PC line. The size of this VOI was generally 75 ± 5 mm, left to right, and 90 ± 5 mm, anterior to posterior. Before the PRESS RF pulses of the water-suppressed scan, the transmitter frequency was changed from the water frequency to the NAA frequency, to eliminate the chemical shift error between the water and NAA VOI. To minimize the inclusion of voxels with chemical shift errors involving other resonances, the outermost rows and columns of the VOI were excluded from analysis.

## SI Data Processing

After zero-filling to 32 × 32 points in $k$-space, applying a Hamming filter with a 50% window width, and 2D spatial Fourier transformation (FT), the time domain SI data were analyzed using LCModel (24). We used the LCModel output statistic on the Cramer-Rao lower bounds of the fit to the peak of interest as a criterion to exclude data of poor quality from the final analysis. If this statistic was greater than 20% for the major peaks of interest, the spectrum was excluded. In the present work, all such peaks (NAA, Ch, and Cr) had Cramer-Rao lower bounds of <20%; thus, no data were excluded. Since the major signals from NAAG are not resolved from those of NAA at 1.5T, and, moreover, are expected to be much less intense than those of NAA (25), we report the combined NAA and NAAG concentration [NAc] in this work. Our experience is that the variability of [NAc] determined by LCModel within a typical 1.5-T SI data set is significantly less than that of [NAA], owing to occasional incorrect discrimination between the NAA and NAAG signal intensities. The results of the LCModel analyses were scaled by a factor determined by analyzing SI data obtained from solutions of either 50 mM NAA or 50 mM Cr. The latter is used to account for any added attenuation of the Cho and Cr signals due to the water-suppression pulses. After small corrections were made for relaxation attenuation (a 10-s TR and 30-ms TE were used in solution experiments), the concentrations determined by LCModel were 8% higher and 2% lower than the known solution concentrations of NAA and Cr, respectively. The NAc, Cho, and Cr results from LCModel were then corrected using Eq. [8]. The relaxation times used for the various relaxation attenuation factors were taken from published reports (GM water: $T_1 = 1.304$, $T_2 = 0.093$ (20); WM water: $T_1 = 0.660$, $T_2 = 0.073$ (20,22); CSF: $T_1 = 2.93$, $T_2 = 0.23$ (22); NAc: $T_1 = 1.28$, $T_2 = 0.34$ (26); Ch: $T_1 = 1.09$, $T_2 = 0.35$ (26); and Cr: $T_1 = 1.09$, $T_2 = 0.35$ (26)).

## Image Segmentation

We examined the performance of three freely available automated segmentation routines to classify GM, WM, and CSF fractions based on the $T_1$ and/or $T_2$ images spanning the SI slice: 1) a K-means algorithm implemented by the IMGCON software (www.fmrib.ox.ac.uk), 2) SPM2's cluster analysis software (www.fil.ion.ucl.ac.uk/spm), and 3) FSL's FAST expectation-maximization routine (www.fmrib.ox.ac.uk/fsl/fast). Before segmentation by K-means or FSL, the brain was extracted using FSL's BET software. All images were corrected for bias field inhomogeneities. Only the FAST and IMGCON (K-means) routines had the capability of performing multispectral segmentation. The segmentation bitmaps were registered to the SI data to correct for any in-plane shift of the SI FOV from the anatomic image FOV during the positioning of the SI VOI.

## Convolution of Segmented Images With the SI PSF

To fully account for the partial volumes of each tissue and CSF fraction in each SI voxel, the segmentation bitmaps from the image slices spanning the SI slab were smoothed to the same effective resolution as the SI data. This was accomplished by convolving the maps with the PSF of the SI data. To do this in a computationally efficient way, we used the convolution theorem. First we applied an inverse FT to the individual GM, WM, and CSF segmentation maps. We then multiplied each of these $k$-space data matrices by a matrix that is the inverse FT of the SI PSF at the resolution of the $k$-space matrix. Next we applied an FT to this product to obtain a segmented image that was smoothed to the effective resolution of the circularly phase-encoded and Hamming-filtered SI acquisition of the study. For SI data without spatial filtering, the inverse FT of the SI PSF is a matrix of ones—either rectangular or elliptical, depending on the phase-encoding method—that is centered in a matrix of zeros at the resolution of the segmented image. In the present work, the FT of the SI PSF was constructed as a Hamming function (used as the spatial filter for the SI data) with radius 24, normalized to a peak amplitude of 1, and centered in a 192 × 192 matrix of zeros. Finally, to obtain the fractional GM, WM, and CSF in each SI voxel, we summed and normalized the pixel values of the smoothed maps over the volume of each SI voxel for each tissue and CSF class. All of the steps outlined above, along with the in-plane registration step, were performed with a program developed in MATLAB® 6.5.1 (The MathWorks, Inc.).

Table 1
Summary of Results of Regression Analyses on Both Pooled and Individual Subject Data Sets*

| Method | Pooled data [NAA] (mM) | | Individual subject data [NAA] $\pm$ SD (mM) | | Inter-subject [NAA] CV | |
|---|---|---|---|---|---|---|
| | GM | WM | GM | WM | GM | WM |
| SPM2 T1 | 19.39 | 13.81 | 19.30 $\pm$ 1.80 | 13.65 $\pm$ 1.43 | 0.09 | 0.10 |
| SPM2 T2 | 16.92 | 14.28 | 16.76 $\pm$ 2.81 | 14.30 $\pm$ 1.35 | 0.17 | 0.10 |
| FAST T1 | 20.54 | 13.87 | 20.55 $\pm$ 2.31 | 13.75 $\pm$ 1.43 | 0.11 | 0.10 |
| FAST T2 | 15.51 | 14.61 | 15.50 $\pm$ 1.60 | 14.51 $\pm$ 1.26 | 0.10 | 0.09 |
| FAST T1/T2 | 17.15 | 14.39 | 17.16 $\pm$ 1.19 | 14.26 $\pm$ 1.38 | 0.07 | 0.10 |
| K-means T1 | 20.32 | 14.01 | 20.08 $\pm$ 2.90 | 13.92 $\pm$ 1.47 | 0.15 | 0.11 |
| K-means T2 | 18.77 | 14.32 | 18.40 $\pm$ 3.34 | 14.30 $\pm$ 1.29 | 0.18 | 0.09 |
| K-means T1/T2 | 18.96 | 14.52 | 18.65 $\pm$ 3.09 | 14.46 $\pm$ 1.37 | 0.17 | 0.09 |
| Total mean | 18.45 | 14.23 | | | | |
| SD | 1.76 | 0.28 | | | | |
| CV | 0.10 | 0.02 | | | | |
| T1 mean | 20.08 | 13.93 | | | | |
| SD | 0.61 | 0.11 | | | | |
| CV | 0.03 | 0.01 | | | | |
| T2 mean | 17.07 | 14.40 | | | | |
| SD | 1.64 | 0.18 | | | | |
| CV | 0.10 | 0.01 | | | | |
| T1/T2 mean | 18.06 | 14.43 | | | | |
| SD | 1.28 | 0.06 | | | | |
| CV | 0.07 | <0.01 | | | | |

*Means, standard deviations (SD), and coefficients of variation (CV) are given for GM and WM NAA concentrations estimated using: 1) all tissue segmentation methods, 2) T1-weighted images only, 3) T2-weighted images only, and 4) both T1- and T2-weighted images (multispectral methods). Also, for each method, means, SDs, and CVs for GM and WM [NAA] estimates across the 14 individual subject data sets of the study are given as a measure of the subject-to-subject variability of a particular method.

## Estimates of Metabolite Concentrations in GM and WM

Linear regression analysis was performed on the metabolite concentration (NAc, Ch, or Cr) and the normalized GM fraction ($f_{GM\_vol}$ / ($f_{GM\_vol}$ + $f_{WM\_vol}$)) for each subject and segmentation method, as well as for the pooled data from all subjects and the segmentation results for each method. Extrapolation of the regression line to 0 or 1 provided an estimate of the metabolite content of pure WM or pure GM, respectively.

## RESULTS

Representative $T_1$- and $T_2$-weighted images and a spectrum from the region of interest in one subject are shown in Fig. 2. Also shown in this figure is the segmentation map generated by FAST using the $T_1$-weighted image of the data set. An example of the regression analysis between [NAc] and normalized GM fraction on the data pooled from all subjects using the partial volume estimates based on FAST multispectral ($T_1/T_2$) segmentation is illustrated in Fig. 3. The influence of the various segmentation approaches on both the pooled and individual subject regression analyses is summarized in Table 1. While the pooled-data estimates of [NAc] in WM ranged by less than $\pm3\%$, from 13.8 mM to 14.6 mM, the estimates of GM [NAc] ranged by $\pm14\%$, from 15.5 mM to 20.5 mM. The greater variability of the latter estimates can be largely attributed to variability in the partial volume estimates of CSF in regions of GM, i.e., along the interhemispheric midline and various sulci. This is illustrated in Fig. 4 for the sample data set shown in Fig. 2, where the estimate of GM [NAc] is shown to correlate strongly ($r^2 = 0.97$) with

the CSF fraction determined in the two columns of spectroscopic voxels along the interhemispheric midline. Generally, partial volume estimates based on $T_1$ image segmentation alone led to higher estimates of NAc in GM ($20.08 \pm 0.61$ mM) than those based on $T_2$ image segmentation alone ($17.07 \pm 1.64$ mM) or on multispectral $T_1$ and $T_2$ image segmentation ($18.06 \pm 1.28$ mM).

Comparisons of the segmentation methods across individual data sets in terms of the coefficient of variation (CV, mean/standard deviation (SD)) of the GM and WM [NAc] estimates revealed that some methods were more consistent than others (Table 1). The variability in WM [NAc] estimates was similar across methods (CV 0.087–0.105),
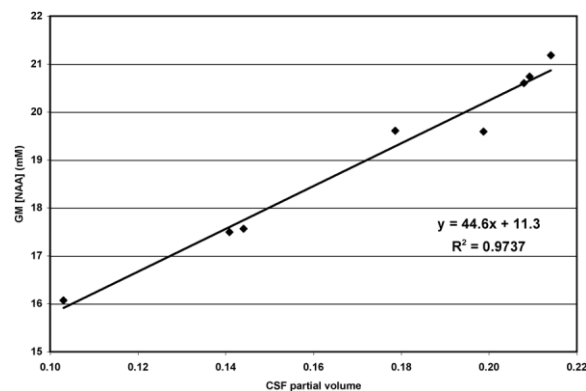
$y = 44.6x + 11.3$
$R^2 = 0.9737$

FIG. 4. Linear regression between the GM [NAA] estimate and the fractional CSF estimate by various segmentation routines for the ROI of one subject (data shown in Fig. 2).

consistent with little CSF being present in WM regions, as discussed above. The variability in GM [NAc] was greatest for all K-means methods (CV = 0.145–0.181) and the SPM2 $T_2$ method (CV = 0.168), while relatively much lower for the SPM2 $T_1$ (CV = 0.093) and FAST methods (CV = 0.069–0.112). The lowest intersubject variability was demonstrated in the estimates based on the FAST multispectral method (CV = 0.069).

Due to its low intersubject variability, FAST multispectral segmentation was also applied to the analysis of Cr and Cho data from all 14 subjects. We note, however, that consistency alone does not validate a method. The "pure" GM and WM mean concentrations and SDs of NAc, Ch, and Cr based on FAST multispectral segmentation and regression analysis on the individual subject data sets were as follows: GM [NAc] = 17.16 ± 1.19 mM; WM [NAc] = 14.26 ± 1.38 mM; GM [Ch] = 3.27 ± 0.47 mM; WM [Ch] = 2.65 ± 0.25 mM; GM [Cr] = 13.98 ± 1.20 mM; and WM [Cr] = 7.10 ± 0.67 mM.

## DISCUSSION

In this report we examine the use of tissue water as an internal concentration reference in SI studies of the brain. A large multicenter study on absolute metabolite quantification using single-voxel MRS, which compared both external reference placement and internal water reference methods, concluded that the internal water method yielded "the most acceptable precision and interlaboratory reproducibility" (27). As in single-voxel MRS studies, the use of internal water in SI studies avoids possible errors in accounting for RF coil inhomogeneity when using external references or ventricle water methods, as well as errors in accounting for coil loading differences when using external reference replacement methods. Furthermore, when SI is used to acquire a reference signal that is not from the same voxel as the metabolites, voxel bleed (determined by the SI PSF) is a factor that may have to be considered. An additional benefit of acquiring the water signal from each voxel is that it can also be used to correct eddy-current distortions of the metabolite line shape and location-dependent chemical shift offsets (28).

However, a number of important caveats must also be considered when using internal water as a reference. Ultimately, the accuracy of the method relies on estimates of the fractional tissue water present, estimates of the various relaxation times associated with this water, and the accuracy of the segmentation method used to measure the tissue and CSF fractions in each spectroscopic voxel. These concerns, of course, apply to single-voxel MRS studies as well as SI, particularly if care is not taken to prescribe "pure" GM or "pure" WM voxels or to acquire the signal with long TRs and short TEs to minimize relaxation effects. Furthermore, accurate segmentation is a requirement for all SI methods that report absolute metabolite concentrations, since, regardless of the concentration reference used, partial volume effects on the metabolite signal intensity must be correctly accounted for.

A thorough discussion of the relative merits of the many image segmentation methods available to spectroscopists is beyond the scope of this paper. However, in general terms, $T_1$ images are considered superior for GM-WM discrimination, $T_2$ images provide a better basis for CSF classification, and multispectral segmentation theoretically takes advantage of both high GM-WM and high GM-CSF contrast images (29,30). Additionally, bias field corrections and/or normalization of the images to a standard template are often applied to improve the performance of the routine. However, a gold standard for brain image segmentation has yet to be established, and, as we have shown here, even relatively sophisticated methods can yield different results. In the current work we found that multispectral segmentation with FSL's FAST routine led to the most consistent estimates of GM [NAc] across the 14 healthy subjects of the study. However, we emphasize again that consistency does not validate a method, and further work is needed to carefully evaluate the different tissue segmentation routines used for SI partial volume corrections in terms of accuracy.

Although numerous reports have described metabolic differences between GM and WM in brain as measured by proton MRS, there is still no consensus on the magnitude and/or direction of these differences. For example, estimates of NAA or NAc in GM in just the last decade have ranged from about 20% less (8) to nearly 50% more (12) than NAA or NAc in WM. The GM/WM [NAc] ratio obtained with internal water as a concentration standard and FAST multispectral segmentation in the present work was 1.20, which is close to the middle of that range. Furthermore, if we assume that 15–30% of the NAc signal in WM derives from NAAG (25), the mean WM concentration of NAA in this study can be estimated to be 10.0–12.1 mM, which is well within the range of <8 mM (12) to >16 mM (16) reported by others (3–9,12,16,25).

In the light of the variety of pulse sequences, concentration standards, and correction factors used for brain MRS, it is clear why most researchers are careful to refer to their measurements of "absolute" metabolite concentrations, or GM/WM differences thereof, only with appropriate caveats. Future SI studies are needed to compare the various commonly-used methods in terms of sources of error, results, and reproducibility, as was done in the multicenter single-voxel MRS study noted above (27). In the present report we examine two of the major sources of error that need to be considered when water is used as an external standard in SI studies. We show that one of these sources of errors, estimates of the different water fraction relaxation times, is relatively minor at short TEs (30 ms). We also demonstrate that different segmentation methods can produce different estimates of the partial volume effect and hence lead to different estimates of metabolite concentrations in GM and WM—a result that has implications for all SI studies involving regional metabolite levels. Nonetheless, these are addressable problems. Images with higher resolution, SNR, and CNR than those obtained in the current work (20.5 min total scan time) might be expected to reduce this variability. While SI studies are usually faced with the problem of balancing the need for image quality with the need to obtain SI data of adequate SNR and resolution, the trend toward higher magnetic fields, multichannel coils, and fast SI sequences should lead to improvements in the typical image quality obtainable in such studies, and hence a reduction in what may be

a major source of variability in the reported data on GM-WM metabolite differences in brain.

## REFERENCES

1. Ernst T, Kreis R, Ross BD. Absolute quantitation of water and metabolites in the human brain. 1: Compartments and water. J Magn Res Ser B 1993;102:1−8.
2. Kreis R, Ernst T, Ross BD. Absolute quantitation of water and metabolites in the human brain. 2: Metabolite concentrations. J Magn Res Ser B 1993;102:9−19.
3. Barker PB, Soher BJ, Blackband SJ, Chatham JC, Mathews VP, Bryan RN. Quantitation of proton NMR spectra of the human brain using tissue water as an internal concentration reference. NMR Biomed 1993; 6:89−94.
4. Christiansen P, Henriksen O, Stubgaard M, Gideon P, Larsson HB. In vivo quantification of brain metabolites by 1H-MRS using water as an internal standard. Magn Reson Imaging 1993;11:107−118.
5. Soher BJ, van Zijl PC, Duyn JH, Barker PB. Quantitative proton MR spectroscopic imaging of the human brain. Magn Reson Med 1996;35: 356−363.
6. McLean MA, Woermann FG, Barker GJ, Duncan JS. Quantitative analysis of short echo time (1)H-MRSI of cerebral gray and white matter. Magn Reson Med 2000;44:401−411.
7. Horska A, Calhoun VD, Bradshaw DH, Barker PB. Rapid method for correction of CSF partial volume in quantitative proton MR spectroscopic imaging. Magn Reson Med 2002;48:555−558.
8. Schuff N, Ezekiel F, Gamst AC, Amend DL, Capizzano AA, Maudsley AA, Weiner MW. Region and tissue differences of metabolites in normally aged brain using multislice 1H magnetic resonance spectroscopic imaging. Magn Reson Med 2001;45:899−907.
9. Hetherington HP, Pan JW, Mason GF, Adams D, Vaughn MJ, Twieg DB, Pohost GM. Quantitative 1H spectroscopic imaging of human brain at 4.1 T using image segmentation. Magn Reson Med 1996;36:21−29.
10. Sharma R, Narayana PA, Wolinsky JS. Grey matter abnormalities in multiple sclerosis: proton magnetic resonance spectroscopic imaging. Mult Scler 2001;7:221−226.
11. Friedman SD, Shaw DW, Artru AA, Richards TL, Gardner J, Dawson G, Posse S, Dager SR. Regional brain chemical alterations in young children with autism spectrum disorder. Neurology 2003;60:100−107.
12. Wang Y, Li SJ. Differentiation of metabolic concentrations between gray matter and white matter of human brain by in vivo 1H magnetic resonance spectroscopy. Magn Reson Med 1998;39:28−33.
13. Chu WJ, Kuzniecky RI, Hugg JW, Abou-Khalil B, Gilliam F, Faught E, Hetherington HP. Statistically driven identification of focal metabolic abnormalities in temporal lobe epilepsy with corrections for tissue heterogeneity using 1H spectroscopic imaging. Magn Reson Med 2000; 43:359−367.
14. Ashburner J, Friston KJ. Nonlinear spatial normalization using basis functions. Hum Brain Mapp 1999;7:254−266.
15. Zhang Y, Brady M, Smith S. Segmentation of brain MR images through a hidden Markov random field model and the expectation-maximization algorithm. IEEE Trans Med Imaging 2001;20:45−57.
16. Knight-Scott J, Haley AP, Rossmiller SR, Farace E, Mai VM, Christopher JM, Manning CA, Simnad VI, Siragy HM. Molality as a unit of measure for expressing 1H MRS brain metabolite concentrations in vivo. Magn Reson Imaging 2003;21:787−797.
17. Ethofer T, Mader I, Seeger U, Helms G, Erb M, Grodd W, Ludolph A, Klose U. Comparison of longitudinal metabolite relaxation times in different regions of the human brain at 1.5 and 3 Tesla. Magn Reson Med 2003;50:1296−1301.
18. Traber F, Block W, Lamerichs R, Gieseke J, Schild HH. 1H metabolite relaxation times at 3.0 tesla: measurements of T1 and T2 values in normal brain and determination of regional differences in transverse relaxation. J Magn Reson Imaging 2004;19:537−545.
19. Brief EE, Whittall KP, Li DK, MacKay AL. Proton T2 relaxation of cerebral metabolites of normal human brain over large TE range. NMR Biomed 2005;18:14−18.
20. Vymazal J, Righini A, Brooks RA, Canesi M, Mariani C, Leonardi M, Pezzoli G. T1 and T2 in the brain of healthy subjects, patients with Parkinson disease, and patients with multiple system atrophy: relation to iron content. Radiology 1999;211:489−495.
21. Kingsley PB, Ogg RJ, Reddick WE, Steen RG. Correction of errors caused by imperfect inversion pulses in MR imaging measurement of T1 relaxation times. Magn Reson Imaging 1998;16:1049−1055.
22. Ibrahim MA, Emerson JF, Cotman CW. Magnetic resonance imaging relaxation times and gadolinium-DTPA relaxivity values in human cerebrospinal fluid. Invest Radiol 1998;33:153−162.
23. Nitz WR, Reimer P. Contrast mechanisms in MR imaging. Eur Radiol 1999;9:1032−1046.
24. Provencher SW. Estimation of metabolite concentrations from localized in vivo proton NMR spectra. Magn Reson Med 1993;30:672−679.
25. Pouwels PJ, Frahm J. Differential distribution of NAA and NAAG in human brain as determined by quantitative localized proton MRS. NMR Biomed 1997;10:73−78.
26. Rutgers DR, van der Grond J. Relaxation times of choline, creatine and N-acetyl aspartate in human cerebral white matter at 1.5 T. NMR Biomed 2002;15:215−221.
27. Keevil SF, Barbiroli B, Brooks JC, Cady EB, Canese R, Carlier P, Collins DJ, Gilligan P, Gobbi G, Hennig J, Kugel H, Leach MO, Metzler D, Mlynarik V, Moser E, Newbold MC, Payne GS, Ring P, Roberts JN, Rowland IJ, Thiel T, Tkac I, Topp S, Wittsack HJ, Podo F. Absolute metabolite quantification by in vivo NMR spectroscopy: II. A multicentre trial of protocols for in vivo localised proton studies of human brain. Magn Reson Imaging 1998;16:1093−1106.
28. Klose U. In vivo proton spectroscopy in presence of eddy currents. Magn Reson Med 1990;14:26−30.
29. Clarke LP, Velthuizen RP, Camacho MA, Heine JJ, Vaidyanathan M, Hall LO, Thatcher RW, Silbiger ML. MRI segmentation: methods and applications. Magn Reson Imaging 1995;13:343−368.
30. Bonekamp D, Horska A, Jacobs MA, Arslanoglu A, Barker PB. Fast method for brain image segmentation: application to proton magnetic resonance spectroscopic imaging. Magn Reson Med 2005;54:1268− 1272.